TOMOGRAPHY® RESEARCH ARTICLE

Low-Noise Active Decoupling Circuit and its Application to ^{13}C Cryogenic RF Coils at 3 T

Juan Diego Sanchez-Heredia[1], Esben Søvsø Szocska Hansen[2], Christoffer Laustsen[2], Vitaliy Zhurbenko[1], and Jan Henrik Ardenkjær-Larsen[1]

[1]Department of Electrical Engineering, Technical University of Denmark, Kongens Lyngby, Copenhagen, Denmark and [2]MR Research Centre, Department of Clinical Medicine, Aarhus University, Aarhus, Denmark

Corresponding Author:
Jan Henrik Ardenkjær-Larsen, PhD
Department of Electrical Engineering, Technical University of Denmark, Kongens Lyngby, Copenhagen, Denmark;
E-mail: jhar@elektro.dtu.dk

Key Words: RF coil, SNR, cryogenic, ^{13}C MRI
Abbreviations: Signal-to-noise ratio (SNR), magnetic resonance (MR), magnetic resonance imaging (MRI), radiofrequency (RF), carbon-13 (^{13}C), hydrogen-1 (^{1}H), equivalent series resistance (ESR), vector network analyzer (VNA)

ABSTRACT

We analyze the loss contributions in a small, 50-mm-diameter receive-only coil for carbon-13 (^{13}C) magnetic resonance imaging at 3 T for 3 different circuits, which, including active decoupling, are compared in terms of their Q-factors and signal-to-noise ratio (SNR). The results show that a circuit using unsegmented tuning and split matching capacitors can provide >20% SNR enhancement at room temperature compared with that using more traditional designs. The performance of the proposed circuit was also measured when cryogenically cooled to 105 K, and an additional 1.6-fold SNR enhancement was achieved on a phantom. The enhanced circuit performance is based on the low capacitance needed to match to 50 Ω when coil losses are low, which significantly reduces the proportion of the current flowing through the matching network and therefore minimizes this loss contribution. This effect makes this circuit particularly suitable for receive-only cryogenic coils and/or small coils for low-gamma nuclei.

INTRODUCTION

The sensitivity of the magnetic resonance (MR) detection circuit is one of the most important aspects of a magnetic resonance imaging (MRI) experiment. Signal-to-noise ratio (SNR) improvement allows higher image resolution and/or reduced acquisition time. In an MR experiment, the noise mainly comes from thermal noise of the coil (and electronics), and the sample noise is due to the interaction of radiofrequency (RF) fields with the lossy sample. For proton imaging in humans, often, the sample losses are dominant because of the relatively high Larmor frequency of protons and the subject's (patient) large size. However, increasing attention has been drawn toward imaging of other nuclei with lower Larmor frequencies, emphasizing the importance of coil losses. Carbon-13 (^{13}C) is of particular interest because it is used for hyperpolarized metabolic MR. This is an exciting new method with potential in early diagnosis of disease, staging, and therapy monitoring (1-5).

Following the trend already established for proton imaging, the SNR of ^{13}C imaging can, in principle, also be improved using smaller surface coils in phased arrays or for acceleration with parallel imaging. However, the assumption is that sample-dominated noise can be achieved. Examples of receive-only double-tuned (4-6) and phased-array (7) coils using small surface elements for ^{13}C have already been reported, showing improved performance over detection using bigger-volume coils. However, developing low-loss ^{13}C small surface coils that work in a sample-dominated noise regime to replicate the enhancements provided by surface coils already seen for proton imaging remains a challenge.

At the lower Larmor frequency of ^{13}C (4 times lower than that of hydrogen-1 [^{1}H]), the noise contribution of the coil becomes more significant. One can approximate the SNR of a nuclear magnetic resonance experiment, in terms of coil and sample losses, as it is done in Styles et al.'s study (8) and calculated using the following equation:

$$SNR \approx \frac{\omega \cdot B_1^-}{\sqrt{R_S \cdot T_S + R_C \cdot T_C}} \qquad (1)$$

where R_S and R_C are the equivalent resistances of sample and coil, respectively, T_S and T_C their temperatures, ω the operating frequency, and B_1^- the field per unit current.

In this context, the SNR of the experiment can be further increased by cooling the coil. The resistivity of copper decreases ca. 8 times when cooled to liquid nitrogen temperature (77 K), allowing a potential ~3-fold SNR increase for the case of no sample losses. The SNR gain obtained from cooling then depends on the balance between coil and sample losses, making it difficult to directly compare coils with different geometries and resonance frequencies. The following are some examples found in the literature of Q factors for cryogenic coils similar in size to the ones we will study here:

ISSN 2379-1381 http://dx.doi.org/10.18383/j.tom.2016.00280

(1) A 30-mm-diameter copper coil for ^{39}K at 9.4 T (18.68 MHz), with an unloaded quality factor improvement $Q_{77K}/Q_{290K} = 450/223$ (9).
(2) A 17-mm-diameter copper coil for ^{1}H at 1.5 T (64 MHz) with unloaded $Q_{77K}/Q_{290K} = 260/125$ (10).
(3) A 35-mm-diameter copper twin horseshoe resonator for ^{1}H at 3 T (128 MHz) with unloaded $Q_{77K}/Q_{290K} = 900/300$ (11).

Cryogenic coils, as those mentioned above, are more often used only as receiver coils, whereas the transmission is performed by a separate volume coil that provides better homogeneity. Therefore, an additional circuitry needs to be added to the coil to detune it during the transmission (active decoupling), preventing inhomogeneities created by the current flowing in the receive coil and also protecting the preamplifier. Decoupling between transmitter and receiver coils has traditionally been implemented by adding a PIN diode in series with an inductor, which is chosen to create high impedance together with one of the capacitors within the coil, therefore greatly reducing the current flow (12, 13).

Some thorough studies have been already conducted, quantifying coil losses for proton imaging at different field strengths (14), showing good agreement between predictions and measurements. Here, we focus on the noise contribution of the circuit used to tune, match, and actively decouple receive-only ^{13}C coils at 3 T (32.13 MHz), and show that, at this frequency, the loss contribution of the tuning capacitor(s) can easily be dominant. In this context, we propose a novel active decoupling circuit and compare its performance with that of traditional schemes. The results show that the proposed circuit significantly reduces the losses, particularly for coils with low resistance. Measured Q-factors of up to 793 at 105 K for an unloaded 50-mm copper loop are obtained, showing the potential of this circuit for cryogenic coils.

Theory

The equivalent circuit diagram of a nuclear magnetic resonance experiment can be simplified as shown in Figure 1. If the coil inductance is fixed, the SNR of the experiment is then dependent on the amount of noise present. The balance between coil, sample, and matching network losses depends mainly on the coil size and test frequency, with coil losses being dominant for lower frequencies and smaller sizes. However, it is frequently overlooked that noise source is the matching network, which, particularly for coils with active decoupling, can become very relevant.

In Figure 1 the matching network is shown as a "black box" that transforms the impedance of the coil to 50 Ω (adding a certain amount of losses to R_M). Let's consider instead the circuit shown in Figure 2A (omitting R_s for the moment), which uses a capacitor in parallel to tune the coil. In this case, we have included the losses added by the capacitors, using their equivalent series resistance (ESR) in series with the ideal capacitors. It can be shown (see Supplemental Appendix) that the losses in this circuit are equivalent to the ones shown in Figure 2B, as long as the resistances (R_C, ESR_T, *and* ESR_M) are much lower than the impedances of the components. In that case, the total losses in the resonator can be approximated using the following equation:

$$R_{eq}^{par} = R_C + ESR_T \quad (2)$$

where R_{eq}^{par} is the total resistance in the resonator (parallel tuned), R_C the losses in the loop, ESR_T is the losses in the tuning capacitor, and ESR_M is the losses in the matching capacitor.

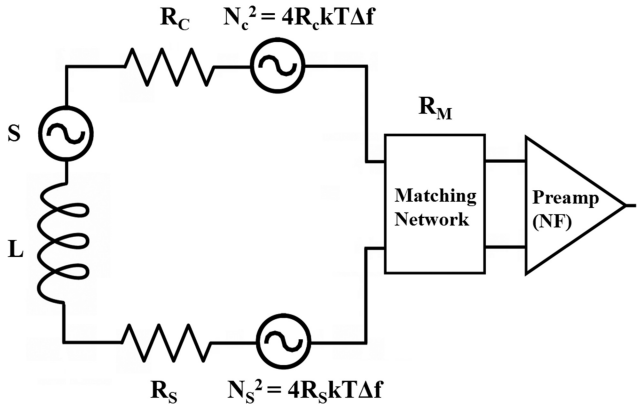

Figure 1. Circuit equivalent of the magnetic resonance imaging (MRI) experiment, including the noise contribution of coil (R_C), sample (R_S), matching network (R_M), and preamp (NF).

For the case of a series tuned coil (as shown in Figure 2C), the total resistance in the resonator can be approximated as that in Figure 2D) (see Supplemental Appendix). Again, this approximation is only valid for coils with equivalent resistance that is much lower than its reactance. Then the total resistance of the series tuned coil (R_{eq}^{ser}) can be expressed using the following equation:

$$R_{eq}^{ser} = R_C + ESR_T + ESR_M \quad (3)$$

Therefore, and to include the capacitor losses in our analysis, for the rest of this study, we will calculate the Q-factor of coils using the following equation:

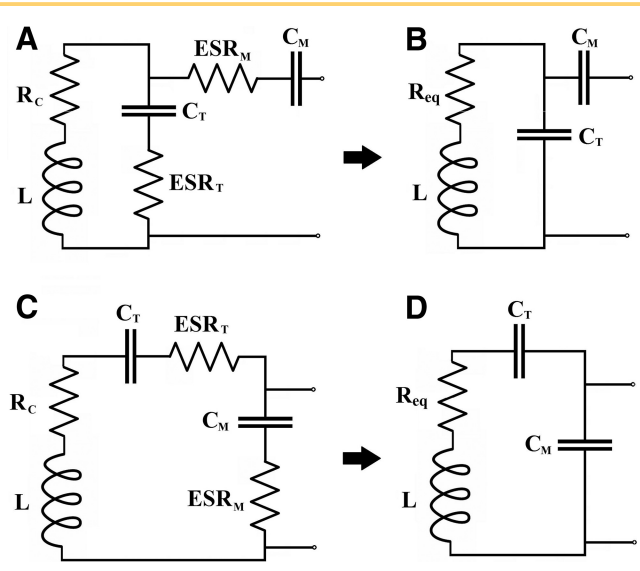

Figure 2. Parallel (A) vs. series (C) tuned coil circuits, and their respective simplified approximations (B)(D).

$$Q = \frac{\omega \cdot L}{R_{eq}} \quad (4)$$

where R_{eq} includes now not only the losses in the loop but also the losses in the capacitors used for tuning and matching [as derived in equations (2) and (3)].

Even though both approximations of R_{eq} are valid for only coils with low losses, their behavior is quite different for the extreme case, where losses tend to zero (Q tends to ∞). In the parallel tuned circuit, lower losses require a lower matching capacitor (higher impedance) to perform the impedance transformation to 50 Ω, which, in practice, reduces the current flowing through this capacitor, minimizing its contribution to the total losses.

For the case of the series tuned coil, lower losses require a higher capacitor for matching (lower impedance), which is problematic because capacitors with higher capacitances have inherently higher losses. In the extreme case where a capacitor with very low impedance (≈mΩ) is needed for matching, the analysis performed here is not valid anymore, and the losses in this capacitor would become dominant. This case is not very realistic though.

A Novel Low-loss Active Decoupling Circuit Using Split Matching Capacitors

There are numerous ways to implement the active decoupling via pole insertion, depending on the particular coil design. Here, the losses of 3 different circuit schemes are compared: the 2 classical (series and parallel tuned coils) and 1 novel, which significantly reduces the losses by using only 1 parallel tuning capacitor.

Figure 3 depicts the 3 receive-only circuit schemes under study. Coil 1 (C_m = 2000 pF, C_t = 470 pF) is a series tuned coil with segmented tuning capacitor, widely used because it allows preamp decoupling schemes (15). In this scheme, the segmenting capacitor is needed to prevent the loop from closing the Direct Current (DC) decoupling circuit. Coil 2 (C_m = 47 pF, C_t = 470 pF) is a parallel tuned coil with 2 balanced matching capacitors and an active decoupling pole formed with one of the tuning capacitors.

Coil 3 (C_m = 22 pF, C_t = 230 pF) is a newly proposed parallel tuned coil with a balanced matching network, where one of the matching capacitors is split and used to create a pole together with the inductor L_1 and the tuning capacitor (opening the loop at the test frequency). The nonsplit matching capacitor is also used to create an additional pole with L_2, which effectively breaks the ground path of the loop and improves the decoupling performance. The values of L_1 and L_2 to create the poles are given by the following equations:

$$L_1 = \frac{1}{\omega^2}\left(\frac{1}{C_t} + \frac{1}{2 \cdot C_m}\right) \quad (5)$$

$$L_2 = \frac{1}{\omega^2 \cdot C_m} \quad (6)$$

As shown in the previous section, the equivalent resistance of a low-loss parallel tuned coil depends on only the losses in the loop and the tuning capacitor. This permits the addition of extra matching capacitors with a minimal effect over the total losses. Therefore, the main advantage of the design proposed for coil 3 is that only 1 tuning capacitor is used to close the loop, thus reducing the resistance added to the resonator. In this case, the loop does not short-circuit the DC decoupling path because of the added split matching capacitor.

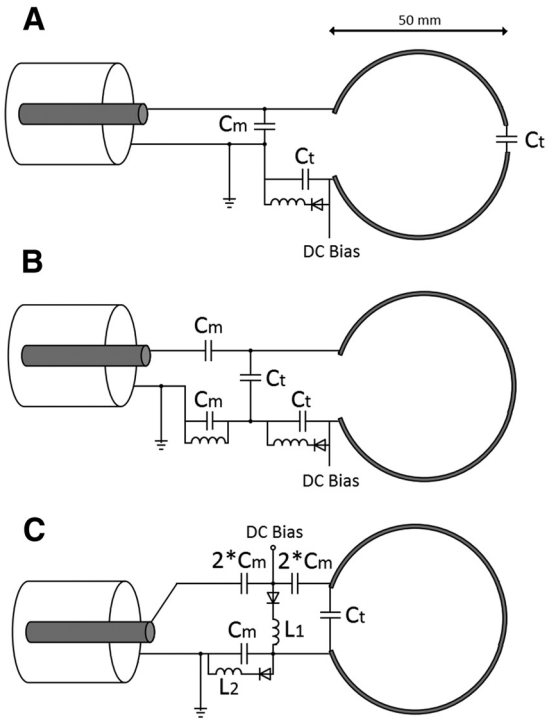

Figure 3. Different coil schemes evaluated in this study: (A) Coil 1: series tuned, (B) Coil 2: parallel tuned, and (C) Coil 3: parallel tuned with split matching capacitor.

METHODS

Coil Geometry

Selecting the right inductance of a receive coil (single loop) is not a trivial task, and it is mainly dependent on the frequency of the experiment and the imaging target depth. A higher inductance provides higher induced signal while reducing the current in the resonator. However, sample losses scale up with the inductance and can be easily dominant, particularly at higher frequencies.

For the case of cryogenic coils, a significant extra reduction of coil losses is made, which can provide an SNR enhancement as long as sample losses are low. Therefore, as sample losses scale with the inductance, there are also reasons to keep the inductance as low as possible. Mispelter et al. (16), in their study, propose a rule of thumb of keeping the coil impedance between 20 and 200 Ω, which seems appropriate for a general case.

In the rest of this study, we will perform our analysis using a (somewhat) arbitrary 50-mm-diameter loop coil, wound with 2.3-mm-thick copper wire. This provides an inductance of ~100 nH (~20 Ω at 32.13 MHz). The main purpose of using this geometry is to use a low-inductance coil, to explore the limits of SNR that can be gained by cooling down a copper coil while keeping sample losses minimal. This coil size is useful for small animal imaging, as it can cover the entire depth of a small rodent, and it also has the potential to be used as a building block for arrays.

The inductance of a 50-mm loop wound with 2.3-mm-thick copper wire can be approximated using the following equation:

$$L = \mu_0 * a * \left[\ln\left(\frac{16a}{d}\right) - 2\right] = 99\,nH \tag{7}$$

Where a is the radius of the loop and d is the diameter of the wire. Its resistance is calculated using the following equation:

$$R_C = \rho\frac{2a}{\delta d} \text{ with } \delta = \sqrt{\frac{2\rho}{\omega\mu_0}} \rightarrow R_C = \frac{a\sqrt{2\rho\omega\mu_0}}{d} = 30\ m\Omega \tag{8}$$

where ρ is the wire resistivity and δ is the skin depth.

Cryostat

For the cryogenic measurements, a simple cryostat was fabricated. The cryostat has the following 2 main parts: a liquid nitrogen deposit enclosed in a Styrofoam isolation and a "cold finger," made of 2 ceramic bars (10 × 10 × 300 mm^3) of aluminum nitride (Precision Ceramics, Birmingham, UK) partially immersed in a liquid nitrogen deposit. The coil is attached to the other end of the ceramic bars with nylon cable ties, and thermally insulated using a coil holder made of Rohacell (Evonik GmbH, Essen, Germany) and a layer of 5 mm of aerogel (Aspen Aerogels Inc., Northborough, MA, USA) placed between the coil and sample.

This setup allows to cool the coil to 105 K in a consistent way, with the 5-mm aerogel layer providing sufficient thermal insulation for >1 hour of experiment without significant thermal transfer to the sample. Therefore, the coil-to-sample distance when the coil is mounted on the cryostat is about 5 mm. For this reason, the measurements at room temperature were done using a 5-mm-thick polytetrafluoroethylene (PTFE) spacer placed between the coil and phantom, to make them comparable. Although this spacing is not necessary at room temperature, it is not the purpose of this study to evaluate the loss of coupling to the sample when extra distance to the coil is included.

Simulation Study

The losses in the 3 actively decoupled coils proposed in Figure 3 were first evaluated via numerical simulations, using a commercial full-wave simulator with its circuit co-simulation (CST Computer Simulation Technology AG, Darmstadt, Germany) feature to add the losses in the lumped elements. The copper conductivity at room temperature and 105 K was taken from Matula et al.'s study (17), with values of 5.96×10^7 and 2.87×10^8 [S/m], respectively. Capacitor losses are modeled using its ESR, which can be calculated from their datasheet, by dividing their reactance at the frequency of interest over the Q-factor. Ceramic capacitors from the CHB series (TEMEX Ceramics, Pessac, France) were used. In this case, we found that capacitors that ranged between 22 and 470 pF have an ESR of about 20 mΩ, whereas capacitors of ≥1000 pF have an ESR of ~40 mΩ. At the time of writing this paper, there were no available data about the ESR of these capacitors at low temperatures; therefore, based on our own characterization, we take the approximation of the ESR that reduces to half when cooled down to liquid nitrogen temperature.

The isolation provided by the diodes used for the active decoupling can potentially play an important role in the total circuit losses. Several nonmagnetic PIN diodes were tested, and finally, MMP7072-128-1 PIN diodes (MACOM, Lowell, MA, USA) were used. The isolation provided by these diodes was measured for 32.13 MHz at room temperature and 105 K, with obtained values of 60 and 120 kΩ, respectively. These values of equivalent resistance were then also included in the simulations to improve their accuracy. Simulations of the unloaded coils without including diode losses were also performed, to determine the importance of these losses relative to the losses in the capacitors.

Simulations were repeated with the coils unloaded (surrounded by free space) and loaded with a spherical phantom emulating the sample placed at a distance of 5 mm from the coil. The phantom is 38 mm in diameter and is filled with muscle simulating liquid as defined by Gabriel et al. (18), which, at 32.13 MHz, has electrical properties, $\varepsilon_r = 87.92$ and $\sigma = 0.686$ [S/m]. The boundary condition was a conductive wall cube 600 mm in length with the coil placed in the center.

Bench Characterization

The coils were then fabricated and characterized in the laboratory. The different active decoupling circuits were mounted on an FR4 printed circuit board etched in house with an appropriate pattern to mount the lumped elements. Because of the relatively high penetration depth at 32.13 MHz (11.7 μm), the printed circuit board with 3 oz (105 μm) copper clad was used. High Q variable capacitors (Johanson Technology Inc., Camarillo, CA, USA) of the 80H85 series where added to allow for fine tuning and matching.

The phantom used to emulate the sample loading is a 38-mm-diameter sphere containing a 1.0M solution of ^{13}C sodium bicarbonate (85 mg/mL) in water. The electrical properties of this solution could not be measured, as the phantom was sealed, but because of the ^{13}C enrichment, it is expected that the conductivity of such a solution will be higher than the nominal values for the muscle simulating liquid described in Gabriel et al.'s study (18).

The coils were first characterized in terms of the unloaded and loaded Q-factor by measuring the reflection coefficient S_{11} with a vector network analyzer (VNA). For a coil matched to 50 Ω, half the power is dissipated at the signal source, so that the Q-factor is given by the following equation:

$$Q = \frac{2 \cdot f_0}{\Delta f_{-3dB}} \tag{9}$$

where Δf_{-3dB} is the −3 dB bandwidth measured from the S_{11} parameter.

The decoupling performance of the coils was also evaluated on the bench using a VNA. The following measurement method is used: a small pickup loop (15 mm in diameter) is placed close to the coil under test (eg, 5 mm). Both coils are then connected to the 2 ports of the VNA, and the transmission coefficient S_{12} is measured for the ON and OFF states of the PIN diodes. The isolation provided by the decoupling circuit is then calculated as the difference in dB between both states.

Scanner Measurements

Imaging experiments were performed using a 3 T clinical scanner (Signa HDx, GE Healthcare, Waukesha, WI, USA), using the phantom described in the previous section. The transmission coil

is a ^{13}C commercially (GE Healthcare, Waukesha, WI, USA) available 60-cm-diameter volume coil, of the clamshell type, previously described in Nelson et al.'s (4) and Tropp et al.'s (19) studies. A single echo time spiral imaging sequence was used with a field of view = 80 × 80 mm, section thickness = 50 mm, and pixel size = 5 mm, similar to the commonly used in vivo spiral imaging sequence used for hyperpolarized examinations (20). Measurements were repeated 32 times, and the obtained images were averaged in magnitude. The total scanning time for the entire sequence, including repetitions, was 32 seconds. The SNR profile, perpendicular to the receiving coil plane, was calculated from the magnitude image as described in Henkelman et al.'s study (21).

All the coils were first connected to a WMA32C low-noise preamplifier (WanTCom, Chanhassen, MN, USA), which has a nominal input impedance of 3 Ω and a measured noise figure at room temperature of 0.7 dB at 32.13 MHz. This preamplifier is not rated for low temperatures, and it was kept at room temperature during the tests where the coils were cryogenically cooled.

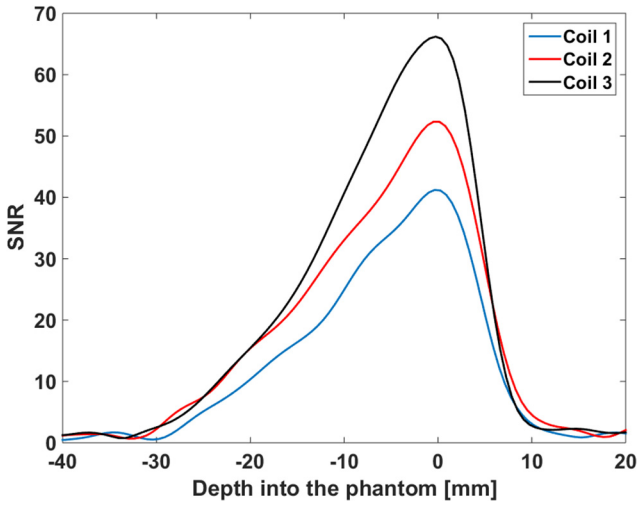

Figure 4. Measured signal-to-noise ratio (SNR) vs. phantom depth for the 3 coils under test at room temperature (290 K).

RESULTS

Room Temperature

The results obtained from the simulations and bench measurements are summarized in Table 1. The coil resistance R_C and inductance L are taken from the electromagnetic simulation, with good agreement with the theoretical equations (7) and (8) for a wire loop. The losses added by the matching network R_M are then calculated from the unloaded Q-factor obtained using the circuit co-simulation, as the difference between the total losses and R_C. The losses added by the sample are calculated as the difference between the losses obtained in the loaded and unloaded simulations. The SNR obtained with each of the coils is shown in Figure 4, averaged over 3 voxels and plotted against the phantom depth.

Active Decoupling Performance

Figure 5 shows the measured active decoupling performance for coil 3, which, at 32.13 MHz, provides a decoupling of 41 dB at room temperature and 48 dB when cooled. The traditional circuits used in coils 1 and 2 provide a better decoupling (see last column of Table 1), and this is because of the Q-factor of the inserted pole. For coils 1 and 2, the pole is made using a tuning capacitor (~470 pF) in parallel with an inductor of ~52 nH. For coil 3, the capacitance of the pole is dominated by the matching capacitors (20–40 pF), which then require much higher inductors (620–1240 nH) in parallel to resonate. These values of inductance are >10 times higher than those used in coils 1 and 2, reducing the Q of these components. This effect is better seen when cooling, as the resistance of the inductors decreases, increasing the Q of the poles and the isolation. Moreover, 40–50 dB of isolation is likely sufficient for most applications, and it is similar to published data from similar experiments (22, 23).

SNR: Room Temperature vs. Cryogenic Temperature

Using the cryostat described before, the Q-factor of the coil was measured, with a ratio of 793/586 obtained between unloaded

Table 1. Coil Parameters Obtained from Simulations and Bench Measurements

		Simulations						Measurements		
	T [K]	L [nH]	R_C [mΩ]	R_M [mΩ]	R_S [mΩ]	Q_U (only capacitors/full circuit)	Q_L	Q_U	Q_L	Active decoupling [dB]
Coil 1		95.2	27	62	3	227/220	209	216	195	62
Coil 2	290	95.2	27	39	3	316/303	286	293	243	62
Coil 3		95.2	27	19	3	435/401	380	390	316	41
Coil 1		94.3	14	37	3	372/371	363	403	341	67
Coil 2	105	94.3	14	19	3	595/584	563	572	464	67
Coil 3		94.3	14	10	3	835/801	756	793	586	48

Abbreviations: L = loop inductance, R_C = loop resistance, R_M = resistance added to the resonator by the circuit elements, R_S = resistance added by the sample (for the loaded case), Q = quality factor of the coil (unloaded and loaded), Active decoupling = difference between the signal transferred from Tx to Rx coil in the ON and OFF states of the circuits (in dB).

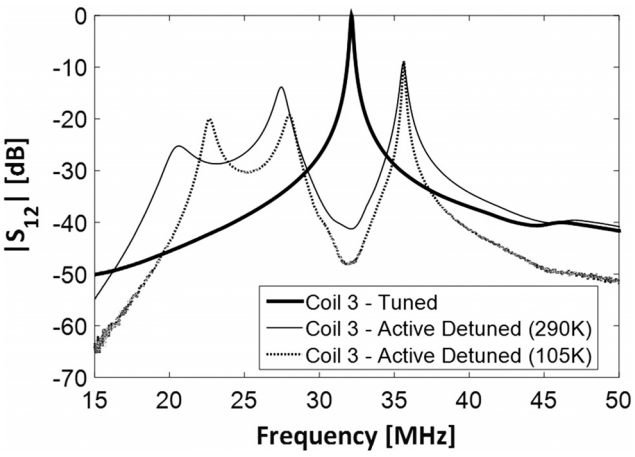

Figure 5. Coil 3 active detuning performance, measured as the normalized transmission coefficient to a loosely coupled pickup loop.

and loaded Q (at 105K). Using these values, we can calculate the expected SNR enhancement when cooling from 290 to 105 K using the following equation:

$$\frac{SNR_{105\,K}}{SNR_{290\,K}} = \sqrt{\frac{\frac{290}{Q_{unloaded\ 290\,K}} + \frac{290}{Q_{loaded\ 290\,K}}}{\frac{105}{Q_{unloaded\ 105\,K}} + \frac{290}{Q_{loaded\ 105\,K}}}} = 1.63$$

To confirm this enhancement, imaging experiments were performed with coil 3 cooled to 105 K using the cryostat described before. Images were then acquired at room temperature and at 105 K, in an otherwise identical setup. The obtained SNR and images are shown in Figure 6, where the expected SNR enhancement is confirmed. This result shows that coil losses are indeed the primary source of noise for this combination of frequency, coil, and sample size.

DISCUSSION

The measured Q-factors for the 3 studied circuits agree well with the simulations for the unloaded case, which shows that the model used for the lumped element losses is reasonable and that the losses in the circuitry are ultimately dominated by the ESR of the capacitors. The extra losses added by the PIN diodes are not very significant in this case as long as PIN diodes with good isolation are used. However, it can be noted that their effect is higher for coil 3 than for the rest, which is explained because of the lower tuning capacitance (higher reactance) required in this circuit, which makes the equivalent parallel resistance of the PIN diode relatively more important. The unsegmented coil (coil 3) showed the largest measured Q-factor in the presence of the sample, confirming that segmentation is not beneficial for the small loop size used here.

The SNR results obtained are consistent and show proportionality to the Q-factor, with coil 3 providing the best SNR (about a 20% improvement compared with coil 2, and almost 40% more than coil 1). The effect of capacitor losses is even more relevant if the thermal losses of the coils are reduced by cryogenically cooling them, accounting for almost half of the total losses for coil 3 when unloaded. The measured Q-factor of the loaded coils is lower than the simulated values, but this can be explained because of the higher conductivity of the ^{13}C-enriched solution compared with the muscle tissue properties described in Gabriel et al.'s study (18).

The results obtained in this study show that for some MRI experiments at lower frequencies, the circuit scheme chosen to drive the coil can have a very important effect on the total losses. When the coil resistance is very low, the losses of the resonator can be easily dominated by the ESR of the tuning capacitor[s]. In this case, it is advantageous to use a parallel tuned scheme and close the loop with only 1 capacitor, such that the resistance added to the resonator is minimized. The reason, as shown in the Supplemental Appendix, is that for such a configuration, the losses in the matching capacitors can be almost neglected. To prevent the loop from shorting the DC decoupling circuit, an extra matching capacitor needs to be added and used to create the tuned trap activated by the decoupling DC signal. The result might be counterintuitive for RF coil designers at higher frequencies, as segmenting the tuning capacitor is one of the most common techniques used to minimize sample losses. The results obtained here show that, depending on the balance between loop, circuit, and sample losses, adding segmenting capacitors may be counterproductive in some cases.

The new coil circuit proposed is particularly useful for cryogenic coils, as the impedance transformation required for parallel tuned coils with very low losses causes dominance of the losses in the tuning capacitor on the losses of the tuning/matching/decoupling network. Here, we have also confirmed this result through bench characterization and imaging experiments on a phantom. An ~1.6-fold SNR improvement at the

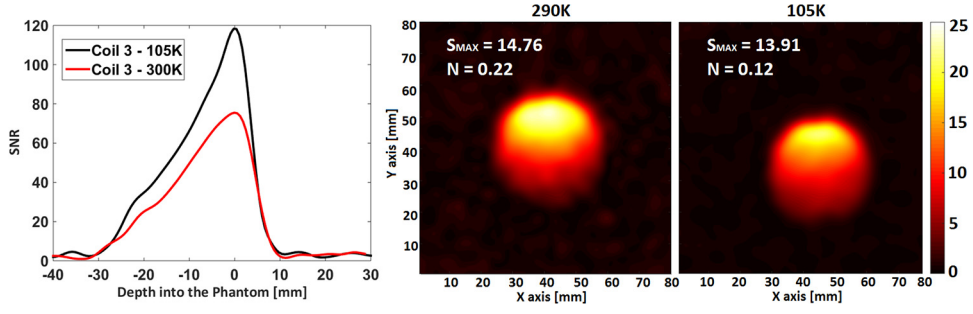

Figure 6. SNR performance of coil 3 at cryogenic temperature (105 K), compared with room temperature (290 K). The signal for the SNR calculations is averaged over 3 pixels of the reconstructed image.

phantom surface was obtained using a 50-mm-diameter loop. This enhancement was obtained even though the sample loss contribution introduced by the phantom was significantly higher than that of the physiological tissue (as shown with the discrepancy of loaded Q-factors in Table 1). Therefore, an even higher enhancement is expected for in vivo experiments.

One shortcoming of this circuit, which may make it unsuitable for some applications, is the lower decoupling due to the losses in the high inductors needed for the poles. We have shown a decoupling of ~40 dB at room temperature compared with that at 60 dB provided by the traditional circuits. For cryogenic coils, this value gets significantly better because of the loss reduction of the matching capacitors and the inductors' resistance, which effectively increase the Q-factor of the poles. Moreover, an isolation over 40 dB may still be enough for most applications, where both transmitting and receiving coils are separated by at least a few centimeters.

CONCLUSION

Given the added complexity and technical difficulties introduced by cryogenic coils for in vivo experiments, it is important to reduce the coil losses to its minimum at room temperature before cryogenically cooling. In this study, an improved circuit scheme for receive-only RF coils is proposed, which significantly reduces the coil losses for coils with very low resistance. For ^{13}C at 3 T, >20% SNR improvement was obtained at room temperature (compared with traditional schemes) using a simple 50-mm-diameter loop (~100 nH). The applicability of this circuit to cryogenic coils is also shown by cryogenically cooling it to 105 K, with an extra ~1.6-fold SNR improvement obtained compared with room temperature. The overall performance of this circuit is based on the assumption of a low-loss coil, which requires very low capacitances for impedance matching. This makes this circuit particularly suitable for cryogenic coils. The SNR improvements of the proposed circuit will be even more noticeable for coils with smaller inductance (lower frequency and/or size).

Supplemental Materials

Supplemental Appendix: http://dx.doi.org/10.18383/j.tom.2016.00280.sup.01

ACKNOWLEDGMENTS

This work has been partly funded by the Danish Council for Independent Research (DFF – 4005-00531) and the Danish National Research Foundation (DNRF124). The authors wish to thank Fraser Robb and his team for many useful discussions and help regarding the imaging experiments.

Disclosures: No disclosures to report.

REFERENCES

1. Ardenkjær-Larsen JH, Fridlund B, Gram A, Hansson G, Hansson L, Lerche MH, Servin R, Thanning M, Golman K. Increase in signal-to-noise ratio of >10,000 times in liquid-state NMR. Proc Natl Acad Sci U S A. 2003;100(18):10158–10163.
2. Golman K, in't Zandt R, Lerche M, Pehrson R, Ardenkjaer-Larsen JH. Metabolic imaging by hyperpolarized 13C magnetic resonance imaging for in vivo tumor diagnosis. Cancer Res. 2006;66(22):10855–10860.
3. Kohler SJ, Yen Y, Wolber J, Chen AP, Albers MJ, Bok R, Zhang V, Tropp J, Nelson S, Vigneron DB, Kurhanewicz J, Hurd . In vivo 13carbon metabolic imaging at 3T with hyperpolarized 13C-1-pyruvate. Magn Reson Med. 2007;58(1):65–69.
4. Nelson SJ, Kurhanewicz J, Vigneron DB, Larson PE, Harzstark AL, Ferrone M, van Criekinge M, Chang JW, Bok R, Park I, Reed G, Carvajal L, Small EJ, Munster P, Weinberg VK, Ardenkjaer-Larsen JH, Chen AP, Hurd RE, Odegardstuen LI, Robb FJ, Tropp J, Murray JA. Metabolic imaging of patients with prostate cancer using hyperpolarized [1-^{13}C]pyruvate. Sci Transl Med. 2013;5(198):198ra108.
5. Park I, Larson PE, Tropp JL, Carvajal L, Reed G, Bok R, Robb F, Bringas J, Kells A, Pivirotto P, Bankiewicz K, Vigneron DB, Nelson SJ. Dynamic hyperpolarized carbon-13 MR metabolic imaging of nonhuman primate brain. Magn Reson Med. 2014;71(1):19–25.
6. Arunachalam A, Whitt D, Fish K, Giaquinto R, Piel J, Watkins R, Hancu I. Accelerated spectroscopic imaging of hyperpolarized C-13 pyruvate using SENSE parallel imaging. NMR Biomed. 2009;22(8):867–873.
7. Cao P, Zhang X, Park I, Najac C, Nelson SJ, Ronen S, Larson PEZ. ^{1}H-^{13}C independently tuned radiofrequency surface coil applied for in vivo hyperpolarized MRI. Magn Reson Med. 2016;76(5):1612–1620.
8. Styles P, Soffe NF, Scott CA, Crag DA, Row F, White DJ, White PCJ. A high-resolution NMR probe in which the coil and preamplifier are cooled with liquid helium. J Magn Reson. 1984;60(3):397–404.
9. Elabyad IA, Kalayciyan R, Shanbhag NC, Schad LR. First in vivo potassium-39 (^{39}K) MRI at 9.4 T using conventional copper radio frequency surface coil cooled to 77 K. IEEE Trans Biomed Eng. 2014;61(2):334–345.
10. Wright AC, Song HK, Wehrli FW. In vivo MR micro imaging with conventional radiofrequency coils cooled to 77 K. Magn Reson Med. 2000;43(2):163–169.
11. Wosik J, Nesteruk K, Kamel MR, Ip F, Xue L, Wright AC, Wehrli FW. Cryogenic Varactor-Tuned 4-element Array and Cryostat for μ-MRI of Trabecular Bone in the Distal Tibia. Paper presented at: 16th Scientific Meeting and Exhibition. The International Society for Magnetic Resonance in Medicine; May 03-09, 2008, Toronto, Ontario.
12. Edelstein WA, Hardy CJ, Mueller OM. Electronic decoupling of surface-coil receivers for NMR imaging and spectroscopy. J Magn Reson. 1986;67(1):156–161.
13. Hyde JS, Rilling RJ, Jesmanowicz ANDA. Passive decoupling of surface coils by pole insertion. J Magn Reson. 1990;89(3):485–495.
14. Kumar A, Edelstein WA, Bottomley PA. Noise figure limits for circular loop MR coils. Magn Reson Med. 2009;61(5):1201–1209.
15. Roemer PB, Edelstein WA, Hayes CE, Souza SP, Mueller OM. The NMR phased array. Magn Reson Med. 1990;16(2):192–225.
16. Mispelter J, Lupu M, Briguet A. NMR Probeheads for Biophysical and Biomedical Experiments: Theoretical Principles & Practical Guidelines. London: Imperial College Press; 2006.
17. Matula RA. Electrical resistivity of copper, gold, palladium, and silver. J Phys Chem Ref Data. 1979;8(4):1147–1298.
18. Gabriel C. Compilation of the dielectric properties of body tissues at RF and microwave frequencies. U.S. Air Force Report AFOSR-TR-96, 1996.
19. Tropp J, Lupo JM, Chen A, Calderon P, McCune D, Grafendorfer T, Ozturk-Isik E, Larson PEZ, Hub S, Yen YF, Robb F, Bok R, Schulte R, Xu D, Hurd R, Vigneron D, Nelson S. Multi-channel metabolic imaging, with SENSE reconstruction, of hyperpolarized [1-(13)C] pyruvate in a live rat at 3.0 tesla on a clinical MR scanner. J Magn Reson. 2011;208(1):171–177.
20. Wiesinger F, Weidl E, Menzel MI, Janich MA, Khegai O, Glaser SJ, Haase A, Schwaiger M, Schulte RF. IDEAL spiral CSI for dynamic metabolic MR imaging of hyperpolarized [1-^{13}C]pyruvate. Magn Reson Med. 2012;68(1):8–16.
21. Henkelman RM. Measurement of signal intensities in the presence of noise in MR images. Med Phys. 1985;12(2):232–233.
22. Keil B, Wiggins GC, Triantafyllou C, Wald LL, Meise FM, Schreiber LM, Klose KJ, Heverhagen JTA. A 20-channel receive-only mouse array coil for a 3 T clinical MRI system. Magn Reson Med. 2011;66(2):582–593.
23. Maunder A, Fallone BG, Daneshmand M, De Zanche N. Experimental verification of SNR and parallel imaging improvements using composite arrays. NMR Biomed. 2015;28(2);141–153.